An ELMO2-RhoG-ILK network modulates microtubule dynamics

Bradley C. Jackson, Iordanka A. Ivanova, and Lina Dagnino
Department of Physiology and Pharmacology, Children's Health Research Institute, and Lawson Health Research Institute, University of Western Ontario, London, ON N6A 5C1, Canada

ABSTRACT ELMO2 belongs to a family of scaffold proteins involved in phagocytosis and cell motility. ELMO2 can simultaneously bind integrin-linked kinase (ILK) and RhoG, forming tripartite ERI complexes. These complexes are involved in promoting β1 integrin–dependent directional migration in undifferentiated epidermal keratinocytes. ELMO2 and ILK have also separately been implicated in microtubule regulation at integrin-containing focal adhesions. During differentiation, epidermal keratinocytes cease to express integrins, but ERI complexes persist. Here we show an integrin-independent role of ERI complexes in modulation of microtubule dynamics in differentiated keratinocytes. Depletion of ERI complexes by inactivating the *Ilk* gene in these cells reduces microtubule growth and increases the frequency of catastrophe. Reciprocally, exogenous expression of ELMO2 or RhoG stabilizes microtubules, but only if ILK is also present. Mechanistically, activation of Rac1 downstream from ERI complexes mediates their effects on microtubule stability. In this pathway, Rac1 serves as a hub to modulate microtubule dynamics through two different routes: 1) phosphorylation and inactivation of the microtubule-destabilizing protein stathmin and 2) phosphorylation and inactivation of GSK-3β, which leads to the activation of CRMP2, promoting microtubule growth. At the cellular level, the absence of ERI species impairs Ca^{2+}-mediated formation of adherens junctions, critical to maintaining mechanical integrity in the epidermis. Our findings support a key role for ERI species in integrin-independent stabilization of the microtubule network in differentiated keratinocytes.

INTRODUCTION

Microtubules are an essential component of the cytoskeleton and are formed by the directional polymerization of αβ-tubulin heterodimers. Microtubules have a slow-growing minus end, which is generally anchored to and stabilized by a microtubule-organizing center. They also have a dynamic, fast-growing plus end, which alternates between periods of growth and shrinkage, separated by catastrophe and rescue events, giving microtubules their characteristic dynamic instability (Rohena and Mooberry, 2014). The regulation of microtubule dynamic instability is critical for many cellular functions, including chromosome segregation, vesicular transport, establishment of cell polarity, and directional cell migration (Rohena and Mooberry, 2014). Many of these processes, however, also require changes in F-actin.

The actin cytoskeleton can also exhibit rapid changes, modulated by multiple proteins, including the Rho family of small GTPases (reviewed in Ridley *et al.*, 2003). Significantly, recent studies suggest that microtubules can also serve as targets for Rho GTPases. Thus these molecules can coordinate global cytoskeletal responses. With regard to microtubules, active Rac1 can indirectly promote the phosphorylation and activation of collapsin response–associated protein 2 (CRMP2), leading to microtubule stabilization, or the inactivation of stathmin, preventing microtubule catastrophe (Gupta *et al.*, 2013; van Haren *et al.*, 2014). Further, directional cell migration

requires the presence of active Rac1 at the leading cell edge, where it regulates actin and microtubule polymerization at lamellipodia (Ridley *et al.*, 2003). In the context of cell migration, Rac1 activation results from the coordinated actions of several signaling pathways, including those associated with complexes that contain engulfment and motility 2 (ELMO2), RhoG, and integrin-linked kinase (ILK; Ho *et al.*, 2009; Ho and Dagnino, 2012b).

ELMO proteins are ubiquitous scaffolds that bridge active RhoG and Dock family proteins to induce Rac1 activation during phagocytosis, endocytic recycling, and neurite outgrowth (Laurin and Cote, 2014). In migrating undifferentiated keratinocytes, active RhoG recruits cytoplasmic species containing ELMO2 and ILK to the cell front, resulting in the formation of a ternary complex in which ELMO2 serves as a bridge between active RhoG and ILK, hereafter termed the ERI complex (Ho *et al.*, 2009; Ho and Dagnino, 2012b). In these cells, the ERI complex is involved in Rac1- and β1 integrin–dependent development of front–rear polarity and cell migration in response to epidermal growth factor, and disruption of this complex by depleting ILK or ELMO2 impairs these processes (Ho *et al.*, 2009; Ho and Dagnino, 2012b). ERI species are also found in terminally differentiated epidermal keratinocytes. However, these cells do not normally migrate, and they exhibit down-regulation of β1 integrin expression upon differentiation. The integrin-independent functions of ERI complexes in terminally differentiated epidermal keratinocytes remain unexplored.

In this study, we examine the involvement of ERI species in the activation of Rac1 pathways in differentiated keratinocytes, which participate in microtubule regulation. We also map signaling events downstream from Rac1 activation that modulate microtubule dynamic instability.

RESULTS

ELMO2 modulation of microtubule stability

ELMO2 forms complexes containing ILK and RhoG, which are involved in β1 integrin–dependent directional migration in undifferentiated keratinocytes (Ho and Dagnino, 2012a). Similar to undifferentiated epidermal keratinocytes in vivo, primary keratinocytes cultured in low-Ca^{2+} growth medium remain undifferentiated and mitotically active; they express abundant integrins and do not assemble adherens or tight junctions (Tu and Bikle, 2013). These cells can be induced to differentiate by culture in medium containing 1.0 mM Ca^{2+} (high-Ca^{2+} medium). Differentiated keratinocytes become quiescent, express differentiation markers, such as involucrin and filaggrin, develop intercellular adherens and tight junctions, and cease to express integrins.

We investigated whether ELMO2 complexes modulate microtubule dynamics in a manner independent of β1 integrin–containing focal adhesions. To this end, we isolated primary keratinocytes from *K14Cre;Ilk$^{f/+}$* epidermis and were able to establish long-term cultures of spontaneously immortalized cells. This keratinocyte line, hereafter termed iKT, exhibits contact inhibition and growth factor dependence, similar to primary epidermal cells (unpublished data). Incubation of iKT cells in high-Ca^{2+} medium for 48 h results in ≥90% inhibition of DNA synthesis and up-regulation of the differentiation markers involucrin and filaggrin in a manner indistinguishable from that in primary wild-type keratinocytes (Figure 1, A and B). On Ca^{2+} addition, iKTs also form adherens and tight junctions, as evidenced by the presence of E-cadherin and zona occludens 1 (ZO-1), respectively, at cell borders (Figure 1D). Of importance, both wild-type and iKT cells exhibit down-regulation of β1 integrins to undetectable levels by 16 h of incubation in high-Ca^{2+} medium (Figure 1, C and D). Thus primary keratinocytes and iKT cells cultured in high-Ca^{2+}

medium constitute suitable models to study biological events in epidermal cells in the absence of major contributions from β1 integrins.

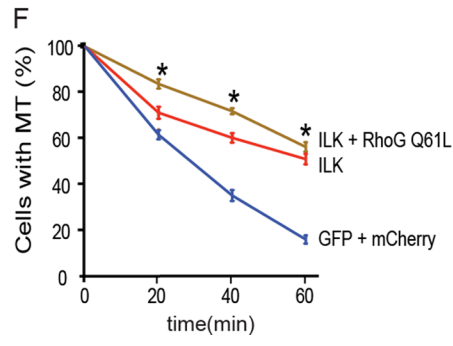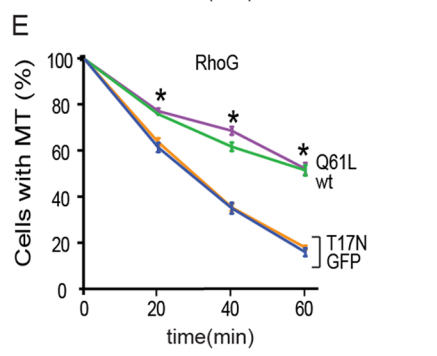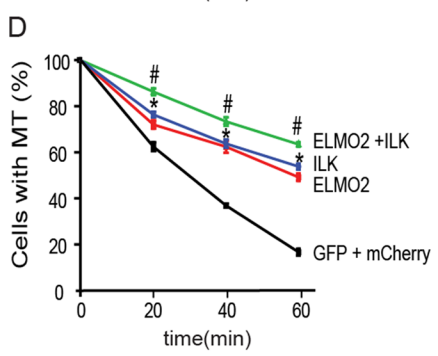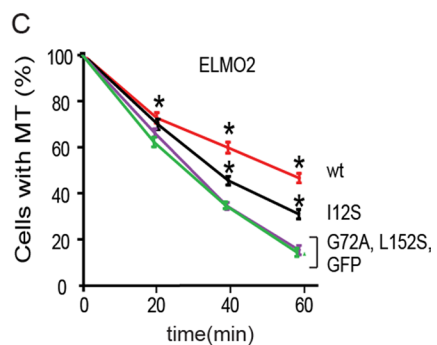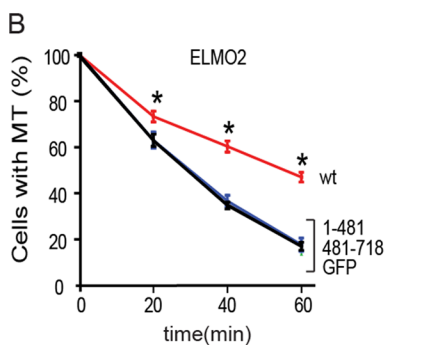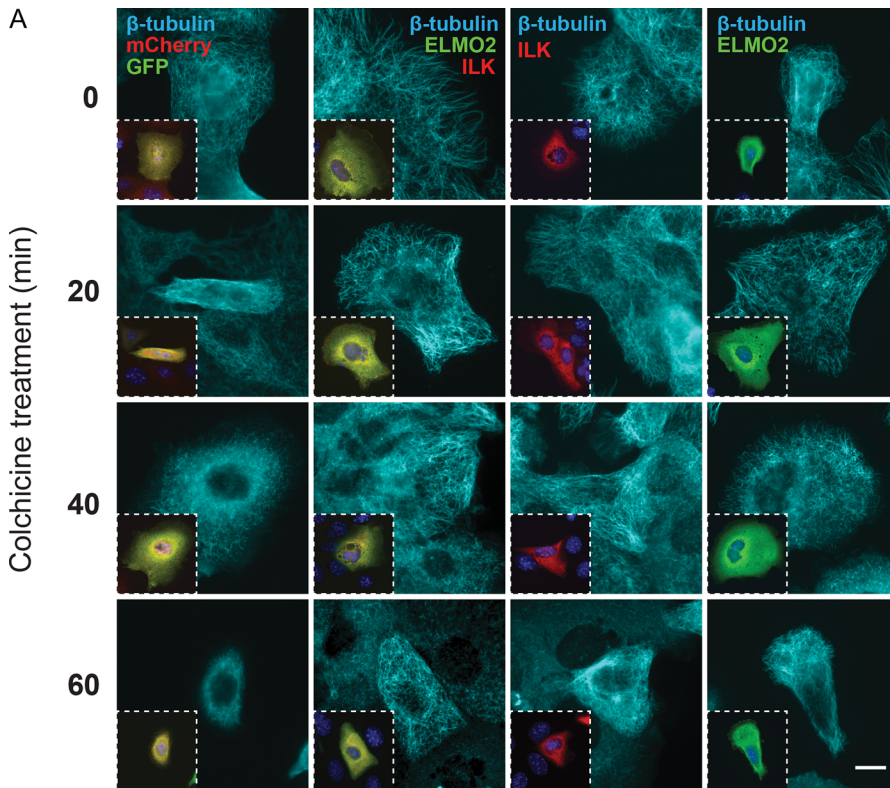To examine the role of ELMO2 in modulating microtubule dynamics, we first investigated whether this protein is able to alter the kinetics of colchicine-induced microtubule disassembly. To this effect, we cultured iKT cells exogenously expressing green fluorescent protein (GFP) or GFP-tagged ELMO2 for 16 h in high-Ca^{2+} medium, followed by incubation in the presence of 5 μM colchicine. At timed intervals after drug addition, we determined the fraction of cells in which we detected at least three microtubules longer than 8 μm, hereafter described as "cells with long microtubules" (Figure 2A). In cells expressing GFP, the interval of culture with colchicine required to reduce the proportion of cells with long microtubules to 50% (which we define here as $t_{1/2}$) was ~28 min. In contrast, almost 70% of ELMO2-expressing cells had long microtubules at this time, and their $t_{1/2}$ was increased twofold, to 60 min (Figure 2B). We next sought to map the regions in ELMO2 important for its microtubule-stabilizing properties. The N-terminus of ELMO2 contains four Armadillo repeats that mediate its interactions with RhoG and ILK (Ho *et al.*, 2009), whereas its C-terminus binds ACF7 and Dock proteins (Margaron *et al.*, 2013; Laurin and Cote, 2014). We exogenously expressed two ELMO2 deletion mutants, composed of amino acid residues 1–481 or 481–718, and observed that neither protein altered the kinetics of microtubule disassembly triggered by colchicine (Figure 2B). These data indicate that intact scaffolding properties in ELMO2 are required for its microtubule-stabilizing activity. To determine whether ELMO2 interactions with ILK and/or RhoG are involved in its microtubule-modulating functions, we also expressed ELMO2 G72A, which does not associate with either RhoG or ILK (Ho *et al.*, 2009). The kinetics of microtubule disassembly in colchicine-treated cells expressing this mutant was indistinguishable from that in cells expressing GFP (Figure 2C). Similar results were obtained with cultures exogenously expressing ELMO2 L152S, which can bind RhoG, but not ILK (Figure 2C). We also assessed microtubule disassembly in cells expressing ELMO2 I12S, which can bind to ILK but not RhoG. Expression of this mutant had a modest but significant effect on microtubule stability, increasing $t_{1/2}$ from 28 to 38 min. Taken together, our data suggest that the ability of ELMO2 to stabilize microtubules in a manner independent of β1 integrins involves its association with RhoG and ILK.

Effect of ILK and RhoG on microtubules

To further examine the hypothesis that ILK and RhoG may function together with ELMO2 to modulate microtubules, we assessed the effect of expressing mCherry-tagged ILK on colchicine-treated iKT cells (Figure 2A). ILK increased $t_{1/2}$ from 28 to >60 min (Figure 2D). Significantly, the joint expression of ELMO2 and ILK further increased microtubule resistance to colchicine, so that 63% of cells exhibited long microtubules after 60 min of incubation with this drug (Figure 2D). Similarly, exogenous expression of wild-type RhoG or the constitutively active RhoG Q61L mutant increased resistance to colchicine and extended $t_{1/2}$ to >60 min, whereas inactive RhoG T17N was without effect (Figure 2E). The joint expression of ILK with either wild-type or Q61L RhoG further enhanced microtubule resistance to colchicine, whereas the kinetics of microtubule disassembly in cells expressing ILK or ILK plus RhoG T17N were identical (Figure 2F; unpublished data). Because ELMO2 is an obligatory bridge between active RhoG and ILK, as the latter two proteins do not directly bind to each other (Ho *et al.*, 2009), our observations are consistent with the proposal that ELMO2-RhoG-ILK (ERI) complexes positively modulate microtubule stability.
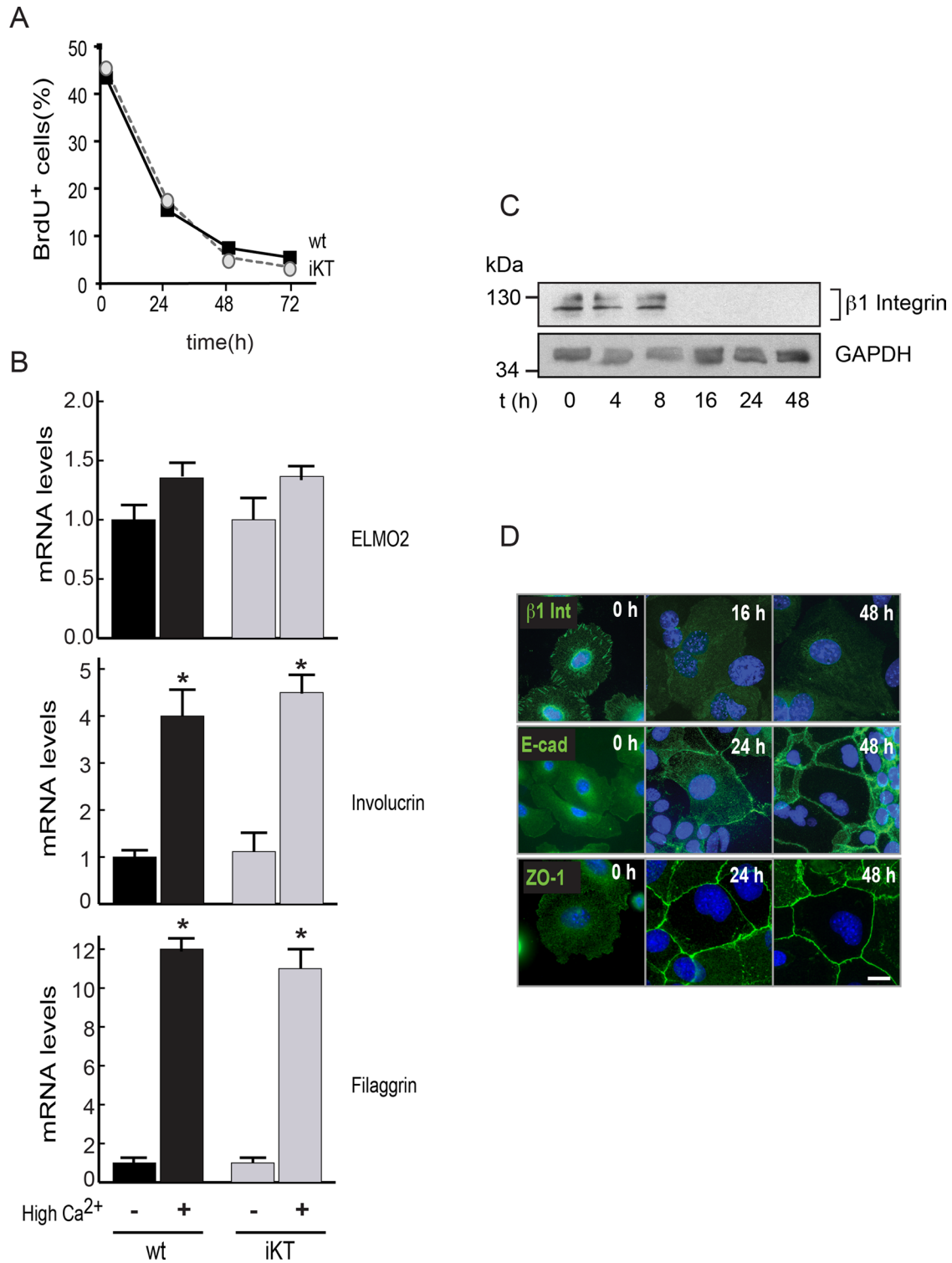
FIGURE 1: Differentiation of iKT keratinocytes by Ca^{2+}. (A) Primary keratinocytes isolated from 2-d-old CD-1 mice (wt) or iKT immortalized keratinocytes were cultured for 2 d in low-Ca^{2+} medium and then switched to high-Ca^{2+} medium. At the indicated times after this switch, BrdU (10 µM, final) was added to the medium, and the cells were processed for immunofluorescence microscopy 2 h later. The fraction of BrdU-positive nuclei was then determined. (B) Total RNA was isolated from primary CD-1 keratinocytes and iKT cells cultured in low- or high-Ca^{2+} medium for 48 h. The relative transcript levels of the indicated genes were then measured by quantitative PCR and normalized to levels of *Rpl6* and *Rps29* mRNA. For each transcript, the data are shown relative to levels in keratinocytes cultured in low-Ca^{2+} medium, which have been set to 1. The results are expressed as the mean + SEM. *$p < 0.05$ relative to values in CD-1 cells cultured in low-Ca^{2+} medium ($n = 3$, ANOVA). (C) Protein lysates were obtained from cells cultured in high-Ca^{2+} medium for the indicated times and were analyzed by immunoblot with the indicated antibodies. GAPDH was used to normalize for protein loading. (D) iKT cells were cultured in high-Ca^{2+} medium for the indicated intervals and processed for immunofluorescence microscopy with antibodies against β1 integrin (β1 int), E-cadherin (E-cad), or ZO-1. Nuclear DNA was visualized with Hoescht 33342. Bar, 12 µm.

FIGURE 2: Stabilization of microtubules by ELMO2, RhoG, and ILK. (A) iKT cells were transfected with vectors encoding proteins indicated on individual panels. Sixteen hours after transfection, the cells were cultured in high-Ca²⁺ medium for an additional 16-h period. Colchicine was then added (5 μM, final), and the cultures were fixed and processed for immunofluorescence microscopy at the indicated intervals after colchicine addition, using anti–β-tubulin antibodies, to visualize and score microtubules. Bar, 12 μm. (B–F) iKT cells were transfected and processed as in A. The graphs represent the percentage of transfected cells that exhibited ≥3 microtubules ≥8 μm in length, and the results are expressed as the mean ± SEM. *$p < 0.05$ relative to values in cultures transfected with GFP (or GFP + mCherry), for each given time point ($n = 3$, ANOVA).
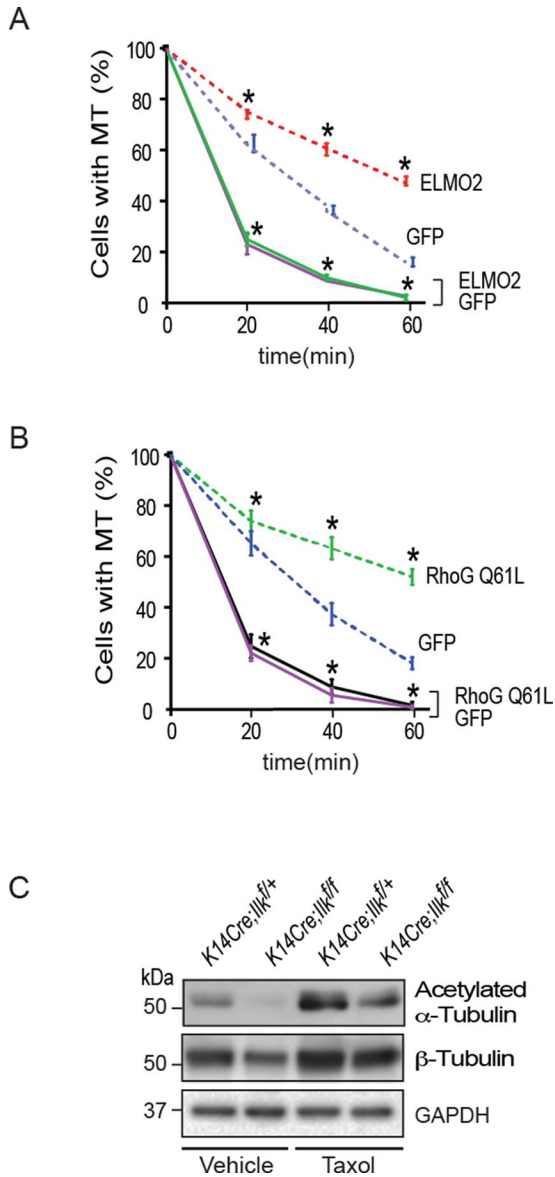
Microtubule dynamic instability in the absence of ERI complexes

To determine the alterations in microtubule dynamics in the absence of ERI complexes, we analyzed primary keratinocytes from *K14Cre;Ilk^{f/f}* mice, with epidermis-restricted inactivation of the *Ilk* gene, and compared them with cells from *K14Cre;Ilk^{f/+}*, ILK-expressing littermates This approach allowed us to conduct experiments in which the cell population studied was devoid of ERI species, with no significant effects on total ELMO2 and RhoG protein levels, which, in ILK-deficient keratinocytes, were comparable to those observed in ILK-expressing cells (Supplemental Figure S1). Because these experiments used cells induced to differentiate with Ca²⁺, this model also allowed us to characterize the role of ERI complexes in microtubule properties without significant contributions from integrin-containing focal adhesions. To validate this model, we exogenously expressed GFP-tagged ELMO2, wild type, or Q61L RhoG in ILK-deficient keratinocytes and established that, in the absence of ILK, none of these proteins protects microtubules from colchicine-induced disassembly (Figure 3, A and B). We conclude that *K14Cre;Ilk^{f/f}* cells constitute an appropriate model to study the effects of disrupting ERI function.

We next examined the role of ERI complexes in intrinsic microtubule properties. Acetylation of α-tubulin occurs primarily in stable microtubules and is increased in the presence of microtubule-stabilizing agents such as paclitaxel (Rohena and Mooberry, 2014). The loss of ERI complexes in ILK-deficient keratinocytes was associated with decreased levels of acetylated α-tubulin (Figure 3C). Treatment of ILK-expressing and ILK-deficient cells with paclitaxel increased acetylated α-tubulin levels by similar magnitudes

FIGURE 3: Effect of ERI complex disruption on microtubule stability. (A, B) $K14Cre;Ilk^{f/+}$, ERI-containing (dashed line), or $K14Cre;Ilk^{f/f}$, ERI-deficient (solid line) primary keratinocytes were transiently transfected with vectors encoding the indicated proteins. Sixteen hours after transfection, the cells were cultured in high-Ca^{2+} medium for 16 h. Colchicine was then added (5 μM, final), and the cultures were fixed and processed for immunofluorescence microscopy at the indicated intervals after colchicine addition. Microtubules were visualized using anti–β-tubulin antibodies. The graphs represent the percentage of transfected cells that exhibited ≥3 microtubules ≥8 μm in length, and the results are expressed as the mean ± SEM. *$p < 0.05$ relative to values in ERI-containing cultures transfected with GFP for each given time point ($n = 3$, ANOVA). (C) ($K14Cre;Ilk^{f/+}$ or $K14Cre;Ilk^{f/f}$ primary keratinocytes were cultured in high-Ca^{2+} medium for 16 h, followed by incubation in the presence of vehicle or paclitaxel (1 μM, final) for 1 h. Cell lysates were prepared and analyzed by immunoblot with the indicated antibodies. GAPDH was used to normalize for protein loading.

(Figure 3C), indicating that, in the absence of intact ERI complexes, the abundance of stable microtubules is diminished.
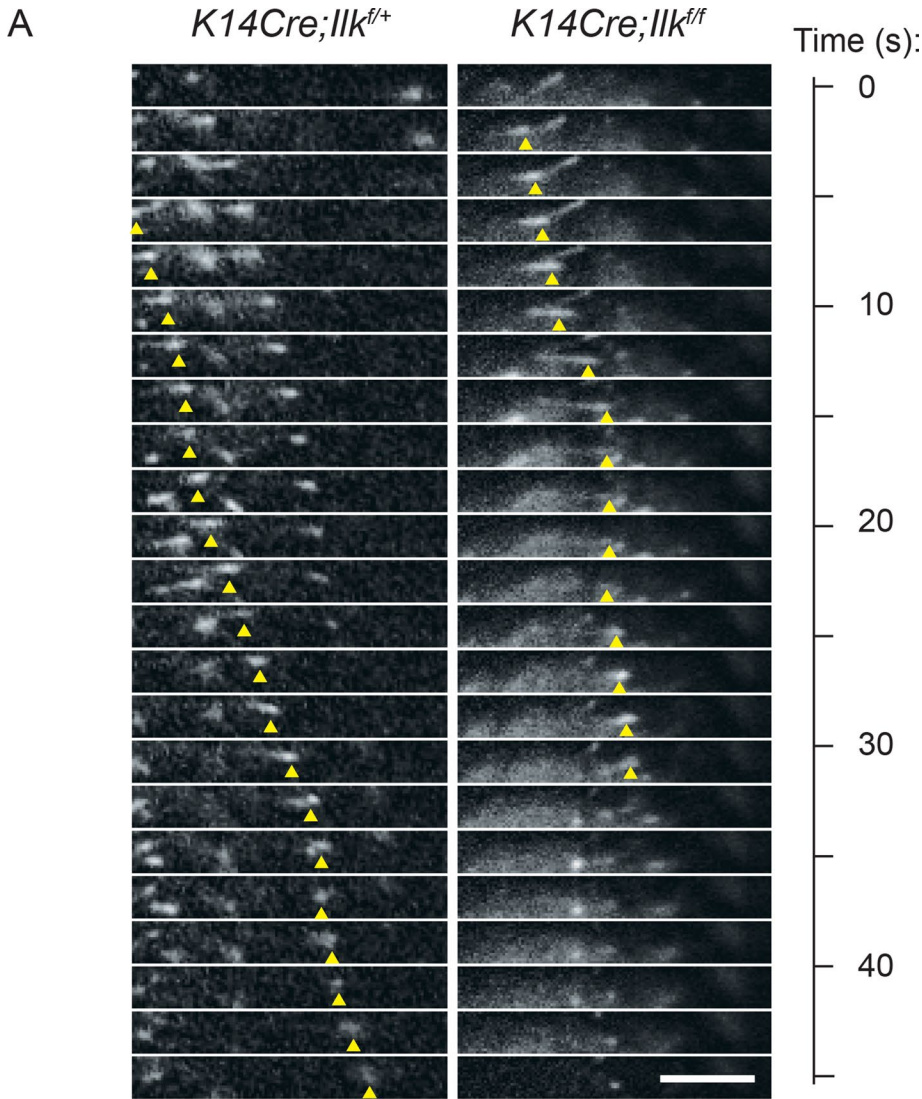
A key property of microtubules is their dynamic instability, characterized by a constant shift between growth and shrinkage

(Straube, 2011). Therefore we next investigated whether the loss of ERI alters the growth and/or shrinkage properties of microtubules. To this end, we exogenously expressed GFP-tagged end binding 1 (EB1) in differentiated $K14Cre;Ilk^{f/+}$ and $K14Cre;Ilk^{f/f}$ keratinocytes. We then obtained time-lapse fluorescence micrographs to record microtubule plus-end growth, as indicated by GFP-EB1 fluorescence (Supplemental Videos S1 and S2). To better visualize microtubule tracks, we also generated maximum intensity projections from time-lapse video images (Figure 4A). We noticed that in ERI-containing cells, microtubule tracks extended from perinuclear areas to regions adjacent to the plasma membrane. In stark contrast, microtubule tracks in ERI-deficient cells failed to reach cell borders. Further image analysis yielded estimates of rate, duration, and length of microtubule growth and frequency of catastrophe (Figure 4B). Although the growth rate was similar in both cell types, microtubule growth duration and track length were ~1.6-fold lower in ERI-deficient cells. Further, catastrophe frequency was about twofold higher in the absence of ERI. Thus, in the absence of ILK and ERI complexes, sustained microtubule growth is severely impaired.

Role of Rac1 and glycogen synthase kinase 3β in modulation of microtubule stability
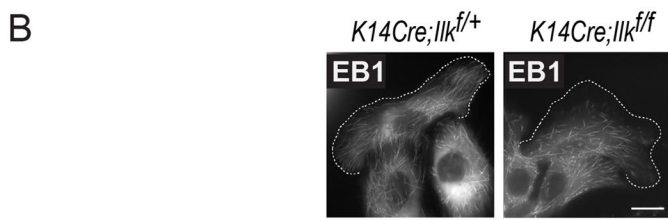
Rac1 is a downstream effector of ILK, ELMO2, and RhoG complexes. Significantly, Rac1 fails to become activated in ERI-deficient keratinocytes under a variety of circumstances, including stimulation by keratinocyte or epidermal growth factor, and under conditions that would normally stimulate directional migration (Katoh and Negishi, 2003; Ho and Dagnino, 2012a; Sayedyahossein et al., 2012, 2014). To investigate whether Rac1 modifies microtubule susceptibility to colchicine, we exogenously expressed GFP-tagged wild-type and G12V constitutively active Rac1 proteins in cells treated with this drug. We observed $t_{1/2} \approx 55$ min in Rac1-expressing cultures, whereas keratinocytes expressing either GFP or inactive Rac1 T17N exhibited $t_{1/2} \approx 28$ min (Figure 5A; unpublished data). Of note, $t_{1/2}$ values were ~16 min in ERI-deficient cells expressing either GFP or wild-type Rac1 (Figure 5A). However, the presence of Rac G12V stabilized microtubules in ERI-deficient cells, increasing $t_{1/2}$ to ~28 min (Figure 5A). These data indicate that Rac1 activation occurs downstream from ILK and ERI complexes and that the presence of Rac1 G12V can at least partially bypass the requirement for these complexes for normal microtubule stability.

Rac1 and Dock3 contribute to microtubule assembly during axonal outgrowth by inhibiting glycogen synthase kinase 3β (GSK-3β; Namekata et al., 2012). Consequently, we investigated whether a link between Rac1 and GSK-3β exists in differentiated keratinocytes. To this end, we exogenously expressed Rac1 proteins in iKT cells and quantified the levels of inactive, phosphorylated GSK-3β. We observed that the presence of wild-type or G12V Rac1 in these cultures increased the abundance of phospho–GSK-3β almost twofold (Figure 5B). Given that normal Rac1 activation requires ILK and ERI species, we reasoned that ILK-deficient cells might exhibit abnormal regulation of GSK-3β. Indeed, we observed reduced levels of inactive, phosphorylated GSK-3β in these cells (Figure 5C). Because the presence of active GSK-3β is associated with decreased microtubule stability, we investigated whether pharmacological inhibition of this kinase restored microtubule resistance to colchicine-induced disassembly in cells lacking ERI complexes. Treatment of normal cells with colchicine in the presence of the GSK-3β inhibitor SB216763 increased the $t_{1/2}$ in normal cells from ~32 to 48 min (Figure 5D). In ERI-deficient keratinocytes, the presence of this drug increased $t_{1/2}$ from 16 to 25 min (Figure 5D). Further, whereas only ~4% of ERI-deficient cells exhibited long microtubules after 40 min of

FIGURE 4: Abnormalities in microtubule dynamics in ERI-deficient keratinocytes. (A) Primary keratinocytes with the indicated genotype were transfected with a vector encoding GFP-labeled EB1. Sixteen hours after transfection, the cells were cultured in high-Ca^{2+} medium for 16 h and imaged by time-lapse videomicroscopy. Individual frames from Supplemental Videos S1 and S2, in which trajectories of individual EB1 comets can be visualized. The yellow arrowheads indicate microtubule tips. Bar, 12 μm. (B) Primary keratinocytes with the indicated genotype were transfected as in A and imaged by time-lapse videomicroscopy. Maximum intensity projections of GFP-EB1 comets were generated from the snapshots in Supplemental Videos S1 and S2 to show GFP-EB1 trajectories in the cell. The images of 20 cells/genotype were analyzed to score 108 comets, which were used to calculate the microtubule dynamics parameters shown in the table. The results represent the mean ± SD ($n = 108$). *$p < 0.0001$ (Student's t test). Dashed lines in the micrographs indicate the plasma membrane. Bar, 12 μm.

incubation with colchicine, the joint presence of SB216763 and colchicine in the growth medium increased the proportion of cells with long microtubules to 38% (Figure 5D). Similar results were obtained with cultures treated with SB415286, a different GSK-3β inhibitor (unpublished data). Thus abnormal levels of active GSK-3β contribute to the observed altered microtubule dynamics in cells lacking ERI species.

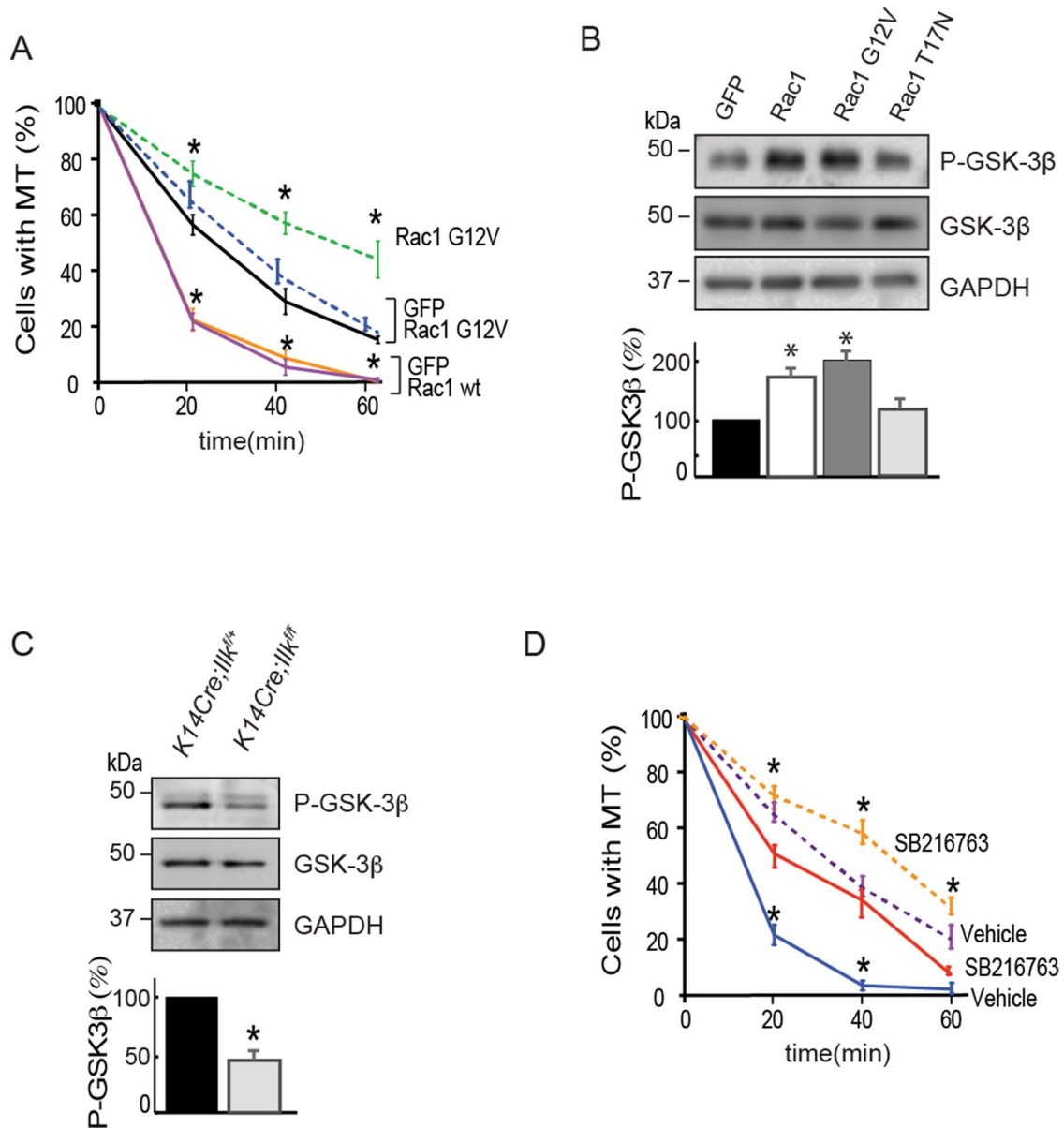GSK-3β phosphorylates CRMP2 on T514, impairing its ability to bind tubulin dimers and stabilize microtubules (Kim et al., 2011). In agreement with the observed reduction in levels of inactive phospho–GSK-3β in ERI-deficient cells, we also observed an increase in CRMP2 phosphorylation (Figure 6A). In neurons, expression of a phosphomimetic CRMP2 T514D mutant inhibits microtubule growth rates (Liz et al., 2014). In contrast, the presence of wild-type or phosphoresistant CRMP2 T514A increases microtubule growth in these cells. Therefore expression of phosphomimetic or phosphoresistant CRMP2 forms would be expected to alter responses to colchicine if CRMP2 is important for microtubule dynamics in keratinocytes. In ERI-expressing cells cultured with colchicine, the presence of CRMP2 T514A increased $t_{1/2}$ from ~40 to 52 min, whereas $t_{1/2}$ in the presence of CRMP2 T514D decreased to ~29 min (Figure 6B). Similarly, CRMP2 T514A imparted microtubule resistance to colchicine in ERI-deficient cells, increasing $t_{1/2}$ from 23 to 40 min (Figure 6C). Conversely, the presence of CRMP2 T514D in these cells decreased $t_{1/2}$ to 10 min. Exogenous expression of wild-type CRMP2 had little effect on microtubule susceptibility to colchicine, irrespective of the presence or absence of ERI species (Figure 6, B and C). Together these observations are consistent with the notion that defective inactivation of GSK-3β and increased CRMP2 phosphorylation

FIGURE 5: Role of Rac1 and GSK-3β in ERI-mediated modulation of microtubules. (A) *K14Cre;Ilk*[f/+] (dashed line) or *K14Cre;Ilk*[f/f] (solid line) primary keratinocytes were transiently transfected with vectors encoding the indicated proteins. Sixteen hours after transfection, the cells were cultured in high-Ca²⁺ medium for 16 h. Colchicine was then added (5 µM, final), and the cultures were fixed and processed for immunofluorescence microscopy at the indicated intervals after colchicine addition. Microtubules were visualized using anti–β-tubulin antibodies. The graphs represent the percentage of transfected cells that exhibited ≥3 microtubules ≥8 µm in length, and the results are expressed as the mean ± SEM. *$p < 0.05$ relative to values in ERI-containing cultures transfected with GFP for each given time point ($n = 3$, ANOVA). (B) *K14Cre;Ilk*[f/+] keratinocytes were transfected with vectors encoding the indicated proteins, and 48 h after transfection, lysates were prepared and analyzed by immunoblot, using antibodies against phosphorylated GSK-3β, total GSK-3β, or GAPDH, used to normalize for protein loading. The histogram shows the average ratio of phospho- to total GSK-3β, measured by densitometric analysis of replicate immunoblots, and is expressed relative to the ratio in GFP-transfected keratinocytes, which is set to 100%. *$p < 0.05$ ($n = 3$, ANOVA). (C) Keratinocytes of the indicated genotypes were cultured in high-Ca²⁺ medium for 16 h, and protein lysates were prepared and analyzed with antibodies against phospho- or total GSK-3β. GAPDH was used to normalize for protein loading. The histogram shows the average ratio of phospho- to total GSK-3β measured by densitometric analysis of replicate immunoblots and is expressed relative to the ratio in *K14Cre;Ilk*[f/+] keratinocytes, which is set to 100%. *$p < 0.05$ ($n = 3$, Student's *t* test). (D) *K14Cre;Ilk*[f/+] (dashed line) or *K14Cre;Ilk*[f/F] (solid line) keratinocytes were cultured in high-Ca²⁺ medium for 16 h and treated with vehicle or SB216763, as described in *Materials and Methods*. Microtubules were visualized as described in A. The results are expressed as the mean ± SEM. *$p < 0.05$ relative to values in ERI-containing cultures transfected with GFP for each given time point ($n = 3$, ANOVA).
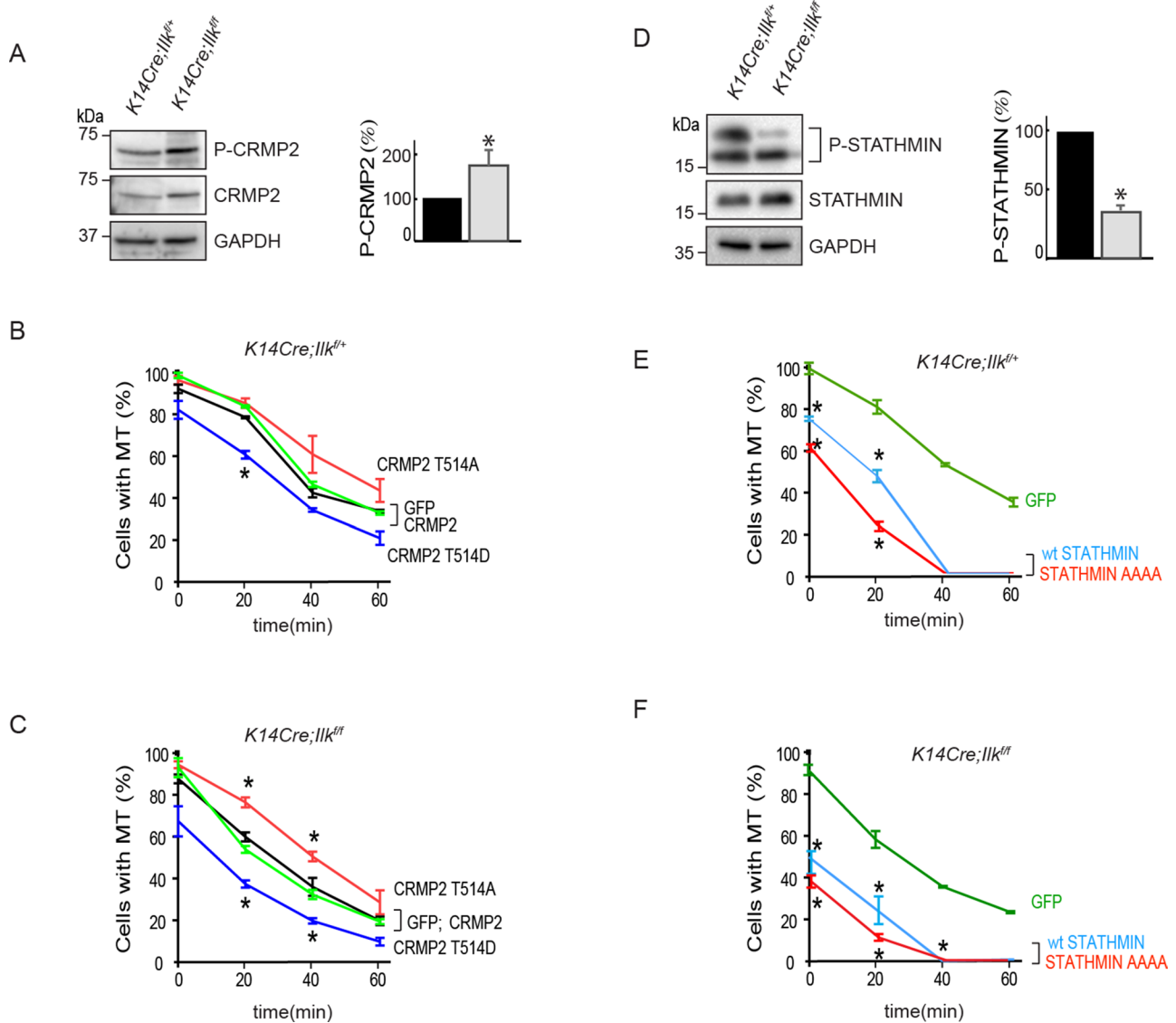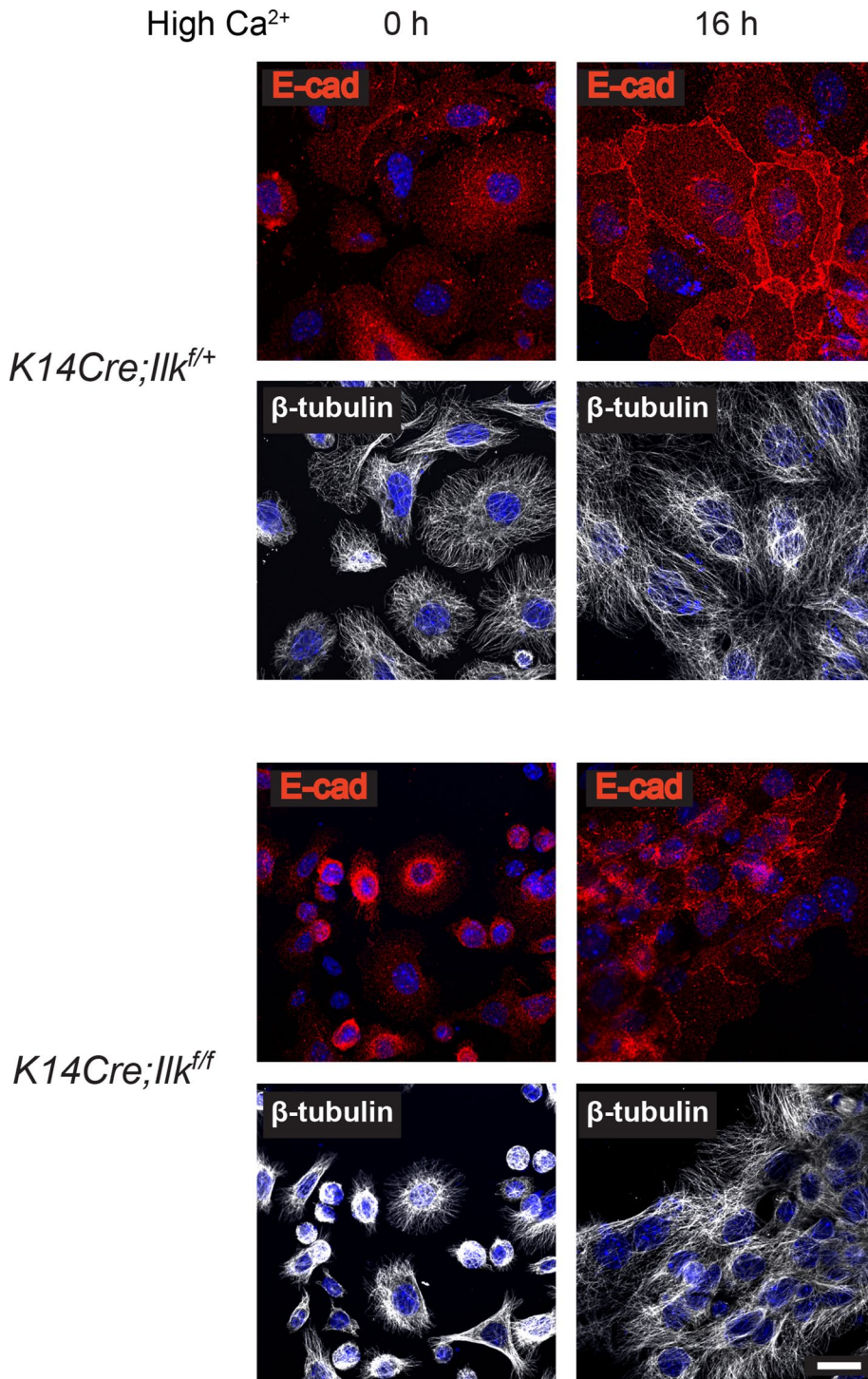
FIGURE 6: CRMP2 and stathmin modulation of microtubules. (A, D) Keratinocytes of the indicated genotypes were cultured in high-Ca^{2+} medium for 16 h, and protein lysates were prepared and analyzed with antibodies against phospho- or total CRMP2, as well as phospho- or total stathmin. GAPDH was used to normalize for protein loading, The histograms show the average ratios of phosphorylated to total proteins as measured by densitometric analysis of replicate immunoblots and are expressed relative to the ratio in *K14Cre;Ilk*$^{f/+}$ keratinocytes, which is set to 100%. *$p < 0.05$ ($n = 3$, Student's t test). (B, C, E, F) *K14Cre;Ilk*$^{f/+}$ or *K14Cre;Ilk*$^{f/f}$ keratinocytes were transiently transfected with vectors encoding the indicated proteins. Sixteen hours after transfection, the cells were cultured in high-Ca^{2+} medium for 16 h. Colchicine was then added (5 µM, final), and the cultures were fixed and processed for immunofluorescence microscopy at the indicated intervals after colchicine addition. Microtubules were visualized using anti–β-tubulin antibodies. The graphs represent the percentage of transfected cells that exhibited at least three microtubules ≥8 µm in length. The results are expressed as the mean ± SEM. *$p < 0.05$ relative to values in GFP-expressing cultures for each given time point ($n = 3$, ANOVA).

contribute to the observed decreased stability of microtubules in the absence of ERI complexes.

Rac1 can also promote the growth of certain subsets of microtubules through a GSK-3β–independent pathway. Specifically, active Rac1 stimulates p21-activated kinase (PAK). PAK then inactivates the microtubule-destabilizing protein stathmin by phosphorylating it, thus reducing the frequency of microtubule catastrophe (Gupta *et al.*, 2013). Hence conditions that reduce Rac1 activation might lead to decreased levels of inactive phospho-stathmin. This, in turn, would increase microtubule destabilization and catastrophe frequency.

Given that ERI complexes are implicated in Rac1 activation, we investigated whether the lower microtubule stability in the absence of these complexes is associated with altered levels of inactive phospho-stathmin. Indeed, we observed that in ERI-deficient keratinocytes, there is a reduced abundance of phosphorylated stathmin, without measurable changes in total stathmin pools (Figure 6D). To further explore the role of stathmin in the modulation of microtubules in keratinocytes, we assessed the consequences of exogenously expressing wild type or a phosphoresistant stathmin mutant that lacks all four serine residues (S16, S25, S38, S63) necessary for inactivation

High Ca²⁺ $\quad$ **0 h** $\quad$ **16 h**

K14Cre;Ilk^{f/+}

E-cad | E-cad
β-tubulin | β-tubulin

K14Cre;Ilk^{f/f}

E-cad | E-cad
β-tubulin | β-tubulin

FIGURE 7: Regulation of E-cadherin subcellular distribution by ILK. Keratinocytes of the indicated genotypes were cultured in high-Ca²⁺ medium for 16 h. The cells were processed for confocal microscopy, using antibodies against E-cadherin (E-cad) and β-tubulin (β-tub). DNA was visualized with Hoescht 33342. Bar, 20 μm.

(wild-type stathmin) or 18 min (stathmin AAAA). Hence stathmin can regulate microtubule dynamics in keratinocytes, likely in a phosphorylation-dependent manner. Consistent with the decreased stability of microtubules in ERI-deficient cells, their susceptibility to additional microtubule perturbation by exogenous stathmin proteins was greatly enhanced compared with that of normal cells. Specifically, the proportion of cells expressing wild-type or stathmin AAAA that had long microtubules in the absence of colchicine was only ~50 and 38%, respectively. This fraction was halved in the presence of colchicine in ~17 min, irrespective of which stathmin form was present (Figure 6F). In these experiments, the $t_{1/2}$ observed in colchicine-treated ERI-deficient cells expressing GFP was 28 min (Figure 6F). Taken together, our observations suggest that stathmin exerts a more pronounced microtubule-destabilizing effect in the absence of ERI complexes.

Abnormal formation of cell–cell contacts in the absence of ERI complexes

In keratinocytes, differentiation induced by elevation of extracellular Ca²⁺ concentrations promotes formation of E-cadherin–based adherens junctions, as well as microtubule reorganization (Sumigray *et al.*, 2012). Specifically, after Ca²⁺ addition, microtubules adopt a noncentrosomal arrangement, forming cortical filaments, which are involved in E-cadherin accumulation at cell–cell contacts (Stehbens *et al.*, 2006). To determine whether the absence of ERI complexes alters the formation of adherens junctions, we analyzed changes in E-cadherin subcellular distribution in differentiating keratinocytes. In agreement with previous reports (Vespa *et al.*, 2005), E-cadherin immunoreactivity is observed in vesicles distributed throughout the cytoplasm in normal keratinocytes cultured in low-Ca²⁺ medium. E-cadherin is found at the plasma membrane after 16 h of culture in high-Ca²⁺ medium, where it forms stable adherens junctions (Figure 7). Under these conditions, rearrangements in microtubule patterns are also observed in response to elevated Ca²⁺, with the microtubule network showing the presence of cortical fibers (Figure 7). E-cadherin–positive vesicles are also observed in undifferentiated ERI-deficient cells, although they appear to concentrate in perinuclear regions (Figure 7). Significantly, during culture in medium with high-Ca²⁺, E-cadherin–containing vesicles remain distributed throughout the cytoplasm, and little or no localization to cell borders is observed, even after 72 h of incubation (Figure 7; unpublished data). Thus adherens junctions fail to form in the absence of ERI complexes, at least within the time frame of these experiments. This emphasizes the importance of ERI species

by phosphorylation (stathmin AAAA; Yip *et al.*, 2014). In ERI-containing cells, overexpression of wild type or stathmin AAAA reduced the proportion of cells with long microtubules by ~25 and 40%, respectively, in the absence of colchicine (Figure 6E). These proteins increased microtubule susceptibility to colchicine, decreasing $t_{1/2}$ from 45 min in GFP-expressing, control cultures to 30 min

in microtubule cytoskeletal rearrangement and establishment of intercellular junctions, critical for the barrier function of the epidermis.

DISCUSSION

We showed that ERI species regulate microtubule assembly and reduce dynamic instability in differentiated epidermal keratinocytes.

Microtubules are organized by multiple mechanisms. For example, undifferentiated keratinocytes in the basal layer of the epidermis have apical centrosomes that function as microtubule-organizing centers (Lechler and Fuchs, 2007). In these and other epithelial cells, β1 integrin adhesion complexes link microtubule plus end–binding proteins with growing microtubules, determining microtubule orientation and resulting in the generation of proper apical-basal polarity (Wickstrom et al., 2010; Akhtar and Streuli, 2013; Lee and Streuli, 2014). In addition, in undifferentiated keratinocytes, ILK recruits IQGAP1 to focal adhesions, resulting in microtubule stabilization at the cell cortex (Wickstrom et al., 2010). These interactions provide a link between the actin cytoskeleton and microtubule regulation, resulting in a net decrease in microtubule dynamic instability. Conversely, focal adhesion turnover requires dynamic microtubules (Stehbens and Wittmann, 2012). A third pathway of microtubule modulation in undifferentiated keratinocytes involves the spectraplakin ACF7, which also participates in coordinately regulating focal adhesion dynamics, F-actin cytoskeleton, and microtubule dynamics (Wu et al., 2008).

In contrast to the established role of focal adhesions in microtubule regulation, few studies have focused on the mechanisms that modulate microtubule dynamics independent of integrins. This has occurred, in part, because integrins are essential for many epithelial cell functions, including survival. Differentiated epidermal keratinocytes, however, constitute a unique, powerful model with which to study this type of microtubule regulation because integrins are not normally expressed in these cells (Watt, 2002).

Differentiation in keratinocytes causes pronounced changes in microtubule organization. For example, centrosomes cease to act as microtubule organizers, and microtubule filaments redistribute to the cell cortex through processes that involve a variety of factors, such as desmoplakin and Lis1 (Sumigray et al., 2011). In particular, desmoplakin can bind the plus end–binding protein EB1, thus modulating microtubule growth at desmosomal cell–cell junctions (Patel et al., 2014).

In differentiated keratinocytes, ELMO2, RhoG, and ILK are found in tripartite ERI complexes (Ho et al., 2009), whose function has remained unexplored. To better understand the role of ERI species in microtubule regulation, we used targeted inactivation of the *Ilk* gene as an efficient means to disrupt ERI complexes. Although three ELMO proteins have been identified in mammals, only ELMO2 associates with ILK (Ho et al., 2009). Thus major impairment of other ELMO isoforms and their RhoG-containing complexes would not be expected to occur in the absence of ILK. Further, the absence of detectable levels of β1 integrins in differentiated keratinocytes also allowed us to study ERI regulation of microtubules without significant potential contributions of β1 integrin–containing focal adhesions.

Collectively several observations in our studies are consistent with a pivotal regulatory role for ERI complexes on microtubule dynamics in differentiated keratinocytes. First, exogenous expression of each individual ERI component protects microtubules from the destabilizing effects of colchicine. Second, the protective effect of ELMO2 and RhoG vis-à-vis colchicine-induced microtubule disassembly is dependent on the presence of ILK. Third, microtubules show increased dynamic instability in ERI-deficient cells.

ELMO2 and ACF7 can associate with each other and modulate microtubule dynamics in various cell types, and ELMO2 knockdown

using RNA interference abolishes the capture of microtubules at the cell cortex in a manner reminiscent of that observed in ERI-deficient keratinocytes (Margaron et al., 2013). Further, ACF7 has been reported to target microtubules to focal adhesions, as well as to link microtubules and F-actin at adherens junctions in keratinocytes (Wu et al., 2008). It will be important to determine whether the modulatory effect of ERI species on microtubules also involves interactions with ACF7.

RhoG has been implicated in microtubule-dependent vesicular transport and neurite outgrowth (Vignal et al., 2001; van Haren et al., 2014). Our data now show that RhoG can decrease colchicine-induced microtubule disassembly and that this property requires the presence of ILK. Because constitutively active RhoG Q61L was not able to restore microtubule resistance to colchicine in ILK-deficient cells, RhoG likely acts jointly with ILK in ERI complexes to modulate microtubule dynamics, although our studies do not exclude the possibility that RhoG also functions upstream from ILK in additional pathways. ILK exerts many of its known functions in association with integrins and focal adhesions. Our work indicates that ILK can also modulate microtubule dynamics through β1 integrin–independent mechanisms, which involve ERI species and, potentially, additional pathways yet to be identified.

The ability of constitutively active Rac1 G12V to protect microtubules from colchicine disassembly in ERI-deficient cells places this GTPase downstream from ERI complexes. Rac1 is also a downstream effector of other factors that regulate microtubule growth, including IQGAP1, Tiam1, and Trio (Tian et al., 2014; van Haren et al., 2014). Thus Rac1 likely functions as a hub to coordinate multiple signaling pathways that ultimately affect microtubule dynamic instability. An important issue for future research is to determine whether any of those microtubule and GTPase modulators work together with ERI species.

In keratinocytes, Rac1 appears to be a common upstream regulator of several microtubule modulatory pathways downstream from ERI species, including GSK-3β/CRMP2. During neurite outgrowth and axonal regeneration, GSK-3β inactivation by Dock3-mediated Rac1 activation enhances microtubule formation via mechanisms that involve CRMP2-mediated extension of plus ends (Ma et al., 2007; Namekata et al., 2012). However, a key unresolved question is whether GSK-3β plays a more global role in regulation of dynamic changes in microtubule stabilization in other tissues. On the basis of the observed protection of microtubules against colchicine-induced disassembly imparted by GSK-3β inhibitors, we now demonstrate an important additional role for this kinase in epidermal cells, independent of the generation of polarized cell extensions or cell movements. Significantly, GSK-3β is involved in many other aspects of epidermal function, including tumorigenesis and hair follicle development (Mill et al., 2005; Ma et al., 2007). Further, the significant increase in microtubule resistance to colchicine observed in ERI-deficient cells expressing phosphoresistant CRMP2 T514A is consistent with the notion that CRMP2 is a key GSK-3β target that participates in the mechanisms that govern microtubule dynamics modulated by ERI species.

Rac1 activation also results in phosphorylation of stathmin, thereby impairing its microtubule catastrophe–promoting properties and modulating keratinocyte forward movements during epidermal repair (Gupta et al., 2013; Schmitt et al., 2013). Phosphorylation of stathmin on four conserved serine residues (S16, S25, S38, S63) is indispensable to completely inhibit its microtubule-destabilizing activity (Honnappa et al., 2006). Our studies with wild-type and gain-of-function stathmin proteins showed their ability to perturb microtubules in normal keratinocytes and emphasized the vulnerability of ERI-deficient cells to microtubule destabilizers.

Although, to the best of our knowledge, loss-of-function stathmin mutants have yet to be described, we would predict that their expression in ERI-deficient cells would result in a decreased frequency of microtubule catastrophe.

A key property of the epidermis is its resistance to mechanical stress, attained in part through development of strong cell–cell adhesions. E-cadherin–based adherens junctions are important for epidermal intercellular adhesion, as their assembly also modulates the formation of tight junctions and desmosomes (Michels et al., 2009). Recently ELMO2 was shown to be essential for the recruitment and spreading of E-cadherin at cell–cell contacts (Toret et al., 2014). In keratinocytes, radial microtubules participate in the establishment of cell–cell junctions, especially early after increases in extracellular Ca^{2+} (Sumigray et al., 2012). In addition, the cortical microtubule network assembled in differentiated keratinocytes is important for the accumulation of E-cadherin at cell borders after Ca^{2+} addition (Stehbens et al., 2006). Cortical microtubules interact with and are necessary for strengthening adherens junctions through mechanisms that involve type II myosin–induced tension (Sumigray et al., 2012). In contrast, cortical microtubules appear to be dispensable for the maintenance of epithelial sheet integrity once junctions are well established (Sumigray et al., 2012). Together these observations provide evidence of the importance of ELMO2 and microtubules in sealing keratinocyte borders, consistent with the disruptions we observed in differentiated ERI-deficient cells, which exhibit both reduced microtubule stability and impaired delivery of E-cadherin to cell borders. An important area for future research will be to examine whether ERI complexes are involved in myosin II modulation of microtubules.

Through the development of a cell model in which the contribution of β1 integrin–containing focal adhesions is minimized, we demonstrated an important and novel regulatory role of ELMO2, RhoG, and ILK in microtubule dynamics. On the basis of our collective observations, we propose a model in which ERI species, possibly localized close to or at the cell cortex, promote Rac1 activation (Figure 8). This event modulates microtubules through at least two
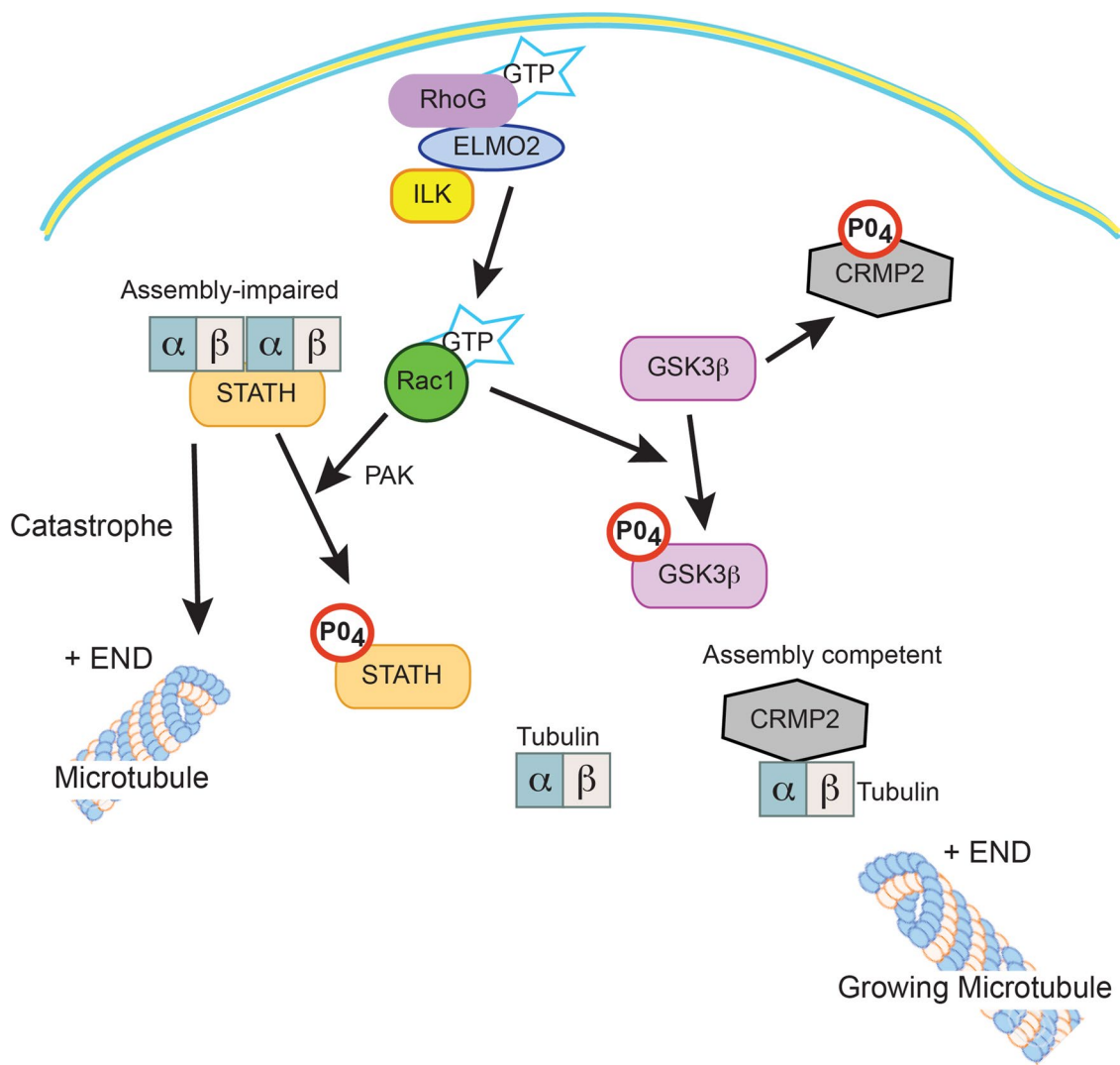
FIGURE 8: Proposed model of ERI complex modulation of microtubules. ERI species localized to regions adjacent to the plasma membrane can promote Rac1 activation. Active, GTP-bound Rac1 in turn mediates activation of kinases that phosphorylate and inactivate the microtubule- destabilizing protein stathmin, reducing microtubule catastrophe events. Rac1 also promotes the phosphorylation and inactivation of GSK-3β. In the presence of inactive GSK-3β, CRMP2 does not get phosphorylated. Unphosphorylated CRMP2 can then bind to tubulin dimers to deliver them to microtubule plus ends, thus promoting microtubule growth.

signaling pathways. In the first pathway, stathmin is phosphorylated, thus abrogating its capacity to sequester αβ-tubulin dimers to promote catastrophe. In the second pathway, Rac1 promotes inactivation of GSK-3β by phosphorylation. Inhibition of GSK-3β, in turn, increases the abundance of unphosphorylated CRMP2. The latter is capable of binding αβ-tubulin dimers, delivering them to the plus ends of growing microtubules. According to this model, ERI complexes may be important determinants to anchor microtubules at the cell cortex. Thus our studies uncovered an unappreciated key signaling pathway that links RhoG, ILK, ELMO2, Rac1, GSK-3β, CRMP2, and stathmin and represent an important advance in the understanding of how microtubules are regulated in epithelial tissues and their potential contribution to mechanical strength in the epidermis.

MATERIALS AND METHODS

Mouse strains

All animal experiments were approved by the University of Western Ontario Animal Use Care Committee (Protocol No. 2007-005-02), in accordance with regulations and guidelines from the Canadian Council on Animal Care. The mouse strain used was CD-1, as well as *K14Cre;Ilk$^{f/+}$* (with ILK-expressing epidermis) and *K14Cre;Ilk$^{f/f}$* (ILK-deficient epidermis), which have been described (Nakrieko *et al.*, 2008b; Rudkouskaya *et al.*, 2013).

Antibodies, reagents, and plasmids

The antibodies used and their sources were as follows: rabbit anti-involucrin (PRB-140C) and rabbit anti-keratin 14 (CLPRB-155P; Covance, Princeton, NJ); mouse anti–E-cadherin (33-4000; Life Technologies, Carlsbad, CA), rabbit anti-mCherry (NBP2-25157; Novus Biochemicals, Littleton, CO), mouse anti–acetylated α-tubulin (T7451; Sigma Aldrich, St. Louis, MO), mouse anti–glyceraldehyde 3-phosphodehydrogenase (GAPDH; ADI-CSA-335; Enzo Life Sciences, Farmingdale, NY); and chicken anti-GFP (ab13970), rabbit anti-ELMO2 (ab181234), rabbit anti-β tubulin (ab6064), and rabbit anti-stathmin (4191P), from Abcam (Cambridge, United Kingdom). The following antibodies were from Cell Signaling Technology (Danvers, MA): rabbit anti–E-cadherin (3591), rabbit anti–phospho-GSK-3β (Ser-9, 9336), mouse anti–GSK-3β (9832), rabbit anti–phospho-CRMP2 (Thr-514, 9397), rabbit anti-CRMP2 (9393), and rabbit anti–phospho-stathmin (Ser-38, 4191P). Mouse anti-RhoG (sc-80015) and mouse anti-c-myc (sc-40) antibodies were from Santa Cruz Biotechnology. The mouse anti-FLAG (F3165) antibody was from Sigma-Aldrich. The mouse anti–5-bromo-2′-deoxyuridine (BrdU; G3G4) monoclonal antibody and the E7 hybridoma that produces anti–β-tubulin immunoglobulin G (IgG), developed by S. J. Kaufman and by M. Klimkowsky, respectively, were obtained from the Developmental Studies Hybridoma Bank, created by the National Institute of Child Health and Human Development of the National Institutes of Health, and maintained at the University of Iowa, Department of Biology (Iowa City, IA). Alexa Fluor 488–, 594–, and 647–conjugated IgG were from Life Technologies.

The GSK-3β inhibitors SB216763 and SB415286 were from Tocris Biosciences (Bristol, United Kingdom); Ca^{2+}-free Eagle's MEM was from Lonza (Walkersville, MD), cholera toxin was from Life Biological Laboratories (Burlington, Canada), rat-tail collagen type I was from BD Biosciences (Bedford, MA), and PhosphoSafe extraction reagent was from EMD Millipore (Billerica, MA). All other reagents were purchased from Sigma-Aldrich or Bioshop (Burlington, Canada).

Mammalian expression vectors encoding mCherry-labeled ILK, as well as GFP-tagged ELMO2, RhoG, and Rac1 proteins, have

been described (Kraynov *et al.*, 2000; Wennerberg *et al.*, 2002; Ho *et al.*, 2009; Ho and Dagnino, 2012b). The plasmid encoding GFP-tagged EB1 was a gift from Tim Mitchison (Harvard University) and Jennifer Tirnauer (Dana-Farber Cancer Institute) and was obtained from Addgene (plasmid # 39299; Cambridge, MA). The vectors encoding wild-type, T514A, and T514D CRMP2 were generous gifts from M. M. Sousa (Instituto de Biologia Molecular e Celular, Porto, Portugal) and have been described (Liz *et al.*, 2014). Vectors encoding wild-type and phosphoresistant stathmin AAAA (Yip *et al.*, 2014) were kind gifts from D.C.H. Ng (University of Melbourne, Melbourne, Australia).

Cell culture, drug treatments, and transfections

Primary keratinocytes were isolated from 2- or 3-d-old mice and cultured in growth medium containing ≤0.05 mM Ca^{2+} (low-Ca^{2+} medium), as described (Dagnino *et al.*, 2010; Sayedyahossein and Dagnino, 2012). iKT cells are a spontaneously immortalized line derived from a primary *K14Cre;Ilk$^{f/+}$* keratinocyte culture. Primary keratinocytes and iKT cells were induced to differentiate by culture in growth medium containing 1 mM Ca^{2+} (high-Ca^{2+} medium) for 16 h. To evaluate BrdU incorporation into DNA, keratinocytes were incubated in high-Ca^{2+} medium in the presence of 10 μM BrdU for 2 h. The cells were fixed in 4% paraformaldehyde and treated with 2 N HCl for 30 min at 22°C to denature the DNA. The cells were then processed for immunofluorescence microscopy as described later. In experiments using GSK-3β inhibitors, cells were treated with either 5 μM SB216763 or 25 μM SB415286 for 24 h before further treatments or processing for analysis, as indicated in individual experiments. Keratinocytes were transiently transfected with polyethyleneimine, as previously described (Nakrieko *et al.*, 2008a; Dagnino *et al.*, 2010).

Microtubule dynamic instability and depolymerization assays

Tracking of microtubule dynamics was conducted with keratinocytes seeded on 35-mm μ-Dish culture plates (81156; Ibidi USA, Madison WI). The cells were transiently transfected with GFP-tagged EB1, and EB1 comets were visualized from time-lapse videomicroscopy images as described (Honore and Braguer, 2011; Straube, 2011). To induce microtubule depolymerization, cells that had been cultured in high-Ca^{2+} medium for 16 h were further cultured in the presence or absence of 5 μM colchicine. At timed intervals after drug addition, the cells were fixed and processed for microscopy.

Fluorescence and confocal microscopy

Cells were fixed with –20°C methanol for 3 min, washed with TBS-TX (50 mM Tris-HCl, pH 7.4, 150 mM NaCl, 0.1% Triton X-100) for 5 min, and incubated with appropriate antibodies as described (Vespa *et al.*, 2005; Rudkouskaya *et al.*, 2013). Fluorescence micrographs and live-cell images were obtained with a Leica DMIRBE fluorescence microscope equipped with an ORCA-ER digital camera (Hamamatsu Photonics, Hamamatsu, Japan), using Volocity 6.1.1 software (Improvision, Coventry, United Kingdom). GFP-EB1 comets were manually tracked using the MTrackJ plug-in for ImageJ (Fiji) software, version 1.48 (Meijering *et al.*, 2012; Schindelin *et al.*, 2012). Microtubule catastrophe frequency and growth rate, duration, and length were calculated as described (Honore and Braguer, 2011). Maximum intensity images were generated by projecting the pixel with the highest intensity at each *xy*-coordinate along the time axis onto a single, two-dimensional image, using the built-in Z-project tool in ImageJ. Kymographs were generated as previously described (Dixit *et al.*, 2009). Confocal analyses were conducted at

the Integrated Microscopy Facility at Biotron, University of Western Ontario (London, Canada). Cell images were acquired with a Plan-Apochromat 63×/1.40 oil differential interference contrast M27 objective mounted on a Zeiss LSM 510 DUO scanning laser confocal microscope, using Zen 2009 SP1 software (Zeiss, Göttingen, Germany).

Immunoblot analysis
Primary keratinocytes were lysed using a modified RIPA buffer (50 mM Tris-HCl, pH 7.4, 150 mM NaCl, 1% NP-40, 0.5% sodium deoxycholate, 1 mM phenylmethylsulfonyl fluoride, 10 mM Na_3VO_4, 1 µg/ml NaF, 1 µg/ml aprotinin, 1 µg/ml pepstatin, and 1 µg/ml leupeptin). For analysis of phosphorylated proteins, cells were lysed in Phosphosafe extraction reagent, as described (Vi *et al.*, 2011). Proteins in the lysates were resolved by denaturing PAGE and transferred to nitrocellulose membranes, which were probed with antibodies indicated in individual experiments. To normalize for protein loading, the blots were also probed for GAPDH.

Statistical analysis
Data were analyzed with GraphPad Prism, version 6.0, software (GraphPad, La Jolla, CA), using Student's *t* test for two-way comparisons or one-way analysis of variance (ANOVA) with Bonferroni posthoc test for multiple comparisons, and significance was set at $p < 0.05$. All experiments were repeated at least three times.

REFERENCES
Akhtar N, Streuli CH (2013). An integrin-ILK-microtubule network orients cell polarity and lumen formation in glandular epithelium. Nat Cell Biol 15, 17–27.

Dagnino L, Ho E, Chang WY (2010). Expression and analysis of exogenous proteins in epidermal cells. Methods Mol Biol 585, 93–105.

Dixit R, Barnett B, Lazarus JE, Tokito M, Goldman YE, Holzbaur EL (2009). Microtubule plus-end tracking by CLIP-170 requires EB1. Proc Natl Acad Sci USA 106, 492–497.

Gupta KK, Li C, Duan A, Alberico EO, Kim OV, Alber MS, Goodson HV (2013). Mechanism for the catastrophe-promoting activity of the microtubule destabilizer Op18/stathmin. Proc Natl Acad Sci USA 110, 20449–20454.

Ho E, Dagnino L (2012a). Emerging role of ILK and ELMO2 in the integration of adhesion and migration pathways. Cell Adh Migr 6, 168–172.

Ho E, Dagnino L (2012b). Epidermal growth factor induction of front-rear polarity and migration in keratinocytes is mediated by integrin-linked kinase and ELMO2. Mol Biol Cell 23, 492–502.

Ho E, Irvine T, Vilk GJ, Lajoie G, Ravichandran KS, D'Souza SJ, Dagnino L (2009). Integrin-linked kinase interactions with ELMO2 modulate cell polarity. Mol Biol Cell 20, 3033–3043.

Honnappa S, Jahnke W, Seelig J, Steinmetz MO (2006). Control of intrinsically disordered stathmin by multisite phosphorylation. J Biol Chem 281, 16078–16083.

Honore S, Braguer D (2011). Investigating microtubule dynamic instability using microtubule-targeting agents. Methods Mol Biol 777, 245–260.

Katoh H, Negishi M (2003). RhoG activates Rac1 by direct interaction with the Dock180-binding protein Elmo. Nature 424, 461–464.

Kim YT, Hur EM, Snider WD, Zhou FQ (2011). Role of GSK3 signaling in neuronal morphogenesis. Front Mol Neurosci 4, 48.

Kraynov VS, Chamberlain C, Bokoch GM, Schwartz MA, Slabaugh S, Hahn KM (2000). Localized Rac activation dynamics visualized in living cells. Science 290, 333–337.

Laurin M, Cote JF (2014). Insights into the biological functions of Dock family guanine nucleotide exchange factors. Genes Dev 28, 533–547.

Lechler T, Fuchs E (2007). Desmoplakin: an unexpected regulator of microtubule organization in the epidermis. J Cell Biol 176, 147–154.

Lee JL, Streuli CH (2014). Integrins and epithelial cell polarity. J Cell Sci 127, 3217–3225.

Liz MA, Mar FM, Santos TE, Pimentel HI, Marques AM, Morgado MM, Vieira S, Sousa VF, Pemble H, Wittmann T, Sutherland C, *et al.* (2014). Neuronal deletion of GSK3beta increases microtubule speed in the growth cone and enhances axon regeneration via CRMP-2 and independently of MAP1B and CLASP2. BMC Biol 12, 47.

Ma C, Wang J, Gao Y, Gao TW, Chen G, Bower KA, Odetallah M, Ding M, Ke Z, Luo J (2007). The role of glycogen synthase kinase 3beta in the transformation of epidermal cells. Cancer Res 67, 7756–7764.

Margaron Y, Fradet N, Cote JF (2013). ELMO recruits actin cross-linking family 7 (ACF7) at the cell membrane for microtubule capture and stabilization of cellular protrusions. J Biol Chem 288, 1184–1199.

Meijering E, Dzyubachyk O, Smal I (2012). Methods for cell and particle tracking. Methods Enzymol 504, 183–200.

Michels C, Aghdam SY, Niessen CM (2009). Cadherin-mediated regulation of tight junctions in stratifying epithelia. Ann NY Acad Sci 1165, 163–168.

Mill P, Mo R, Hu MC, Dagnino L, Rosenblum ND, Hui CC (2005). Shh controls epithelial proliferation via independent pathways that converge on N-Myc. Dev Cell 9, 293–303.

Nakrieko KA, Vespa A, Mason D, Irvine TS, D'Souza SJ, Dagnino L (2008a). Modulation of integrin-linked kinase nucleo-cytoplasmic shuttling by ILKAP and CRM1. Cell Cycle 7, 2157–2166.

Nakrieko KA, Welch I, Dupuis H, Bryce D, Pajak A, St Arnaud R, Dedhar S, D'Souza SJ, Dagnino L (2008b). Impaired hair follicle morphogenesis and polarized keratinocyte movement upon conditional inactivation of integrin-linked kinase in the epidermis. Mol Biol Cell 19, 1462–1473.

Namekata K, Harada C, Guo X, Kimura A, Kittaka D, Watanabe H, Harada T (2012). Dock3 stimulates axonal outgrowth via GSK-3beta-mediated microtubule assembly. J Neurosci 32, 264–274.

Patel DM, Dubash AD, Kreitzer G, Green KJ (2014). Disease mutations in desmoplakin inhibit Cx43 membrane targeting mediated by desmoplakin-EB1 interactions. J Cell Biol 206, 779–797.

Ridley AJ, Schwartz MA, Burridge K, Firtel RA, Ginsberg MH, Borisy G, Parsons JT, Horwitz AR (2003). Cell migration: integrating signals from front to back. Science 302, 1704–1709.

Rohena CC, Mooberry SL (2014). Recent progress with microtubule stabilizers: new compounds, binding modes and cellular activities. Nat Prod Rep 31, 335–355.

Rudkouskaya A, Welch I, Dagnino L (2013). ILK modulates epithelial polarity and matrix formation in hair follicles. Mol Biol Cell 25, 620–632.

Sayedyahossein S, Dagnino L (2012). Integrins and small GTPases as modulators of phagocytosis. Int Rev Cell Mol Biol 302, 321–354.

Sayedyahossein S, Nini L, Irvine TS, Dagnino L (2012). Essential role of integrin-linked kinase in regulation of phagocytosis in keratinocytes. FASEB J 26, 4218–4229.

Sayedyahossein S, Xu SX, Rudkouskaya A, McGavin MJ, McCormick JK, Dagnino L (2014). Staphylococcus aureus keratinocyte invasion is mediated by integrin-linked kinase and Rac1. FASEB J 29, 711–723.

Schindelin J, Arganda-Carreras I, Frise E, Kaynig V, Longair M, Pietzsch T, Preibisch S, Rueden C, Saalfeld S, Schmid B, *et al.* (2012). Fiji: an open-source platform for biological-image analysis. Nat Methods 9, 676–682.

Schmitt S, Safferling K, Westphal K, Hrabowski M, Muller U, Angel P, Wiechert L, Ehemann V, Muller B, Holland-Cunz S, *et al.* (2013). Stathmin regulates keratinocyte proliferation and migration during cutaneous regeneration. PLoS One 8, e75075.

Stehbens SJ, Paterson AD, Crampton MS, Shewan AM, Ferguson C, Akhmanova A, Parton RG, Yap AS (2006). Dynamic microtubules regulate the local concentration of E-cadherin at cell-cell contacts. J Cell Sci 119, 1801–1811.

Stehbens S, Wittmann T (2012). Targeting and transport: how microtubules control focal adhesion dynamics. J Cell Biol 198, 481–489.

Straube A (2011). How to measure microtubule dynamics? Methods Mol Biol 777, 1–14.

Sumigray KD, Chen H, Lechler T (2011). Lis1 is essential for cortical microtubule organization and desmosome stability in the epidermis. J Cell Biol 194, 631–642.

Sumigray KD, Foote HP, Lechler T (2012). Noncentrosomal microtubules and type II myosins potentiate epidermal cell adhesion and barrier formation. J Cell Biol 199, 513–525.

Tian Y, Tian X, Gawlak G, O'Donnell JJ 3rd, Sacks DB, Birukova AA (2014). IQGAP1 regulates endothelial barrier function via EB1-cortactin cross talk. Mol Cell Biol 34, 3546–3558.

Toret CP, Collins C, Nelson WJ (2014). An Elmo-Dock complex locally controls Rho GTPases and actin remodeling during cadherin-mediated adhesion. J Cell Biol 207, 577–587.

Tu CL, Bikle DD (2013). Role of the calcium-sensing receptor in calcium regulation of epidermal differentiation and function. Best Pract Res Clin Endocrinol Metab 27, 415–427.

van Haren J, Boudeau J, Schmidt S, Basu S, Liu Z, Lammers D, Demmers J, Benhari J, Grosveld F, Debant A, Galjart N (2014). Dynamic microtubules catalyze formation of navigator-TRIO complexes to regulate neurite extension. Curr Biol 24, 1778–1785.

Vespa A, D'Souza SJ, Dagnino L (2005). A novel role for integrin-linked kinase in epithelial sheet morphogenesis. Mol Biol Cell 16, 4084–4095.

Vi L, de Lasa C, DiGuglielmo GM, Dagnino L (2011). Integrin-linked kinase is required for TGF-beta1 induction of dermal myofibroblast differentiation. J Invest Dermatol 131, 586–593.

Vignal E, Blangy A, Martin M, Gauthier-Rouviere C, Fort P (2001). Kinectin is a key effector of RhoG microtubule-dependent cellular activity. Mol Cell Biol 21, 8022–8034.

Watt FM (2002). Role of integrins in regulating epidermal adhesion, growth and differentiation. EMBO J 21, 3919–3926.

Wennerberg K, Ellerbroek SM, Liu RY, Karnoub AE, Burridge K, Der CJ (2002). RhoG signals in parallel with Rac1 and Cdc42. J Biol Chem 277, 47810–47817.

Wickstrom SA, Lange A, Hess MW, Polleux J, Spatz JP, Kruger M, Pfaller K, Lambacher A, Bloch W, Mann M, et al. (2010). Integrin-linked kinase controls microtubule dynamics required for plasma membrane targeting of caveolae. Dev Cell 19, 574–588.

Wu X, Kodama A, Fuchs E (2008). ACF7 regulates cytoskeletal-focal adhesion dynamics and migration and has ATPase activity. Cell 135, 137–148.

Yip YY, Yeap YY, Bogoyevitch MA, Ng DC (2014). cAMP-dependent protein kinase and c-Jun N-terminal kinase mediate stathmin phosphorylation for the maintenance of interphase microtubules during osmotic stress. J Biol Chem 289, 2157–2169.